Comparative Study of Oil-Dilution Capability of Dimethyl Ether and Hexane as Steam Additives for Steam-Assisted Gravity Drainage

Kwang Hoon Baek, Kai Sheng, Francisco J. Argüelles-Vivas, and **Ryosuke Okuno,** University of Texas at Austin

Summary

Dimethyl ether (DME) was investigated as a potential additive to steam to improve steam-assisted gravity drainage (SAGD) in a previous simulation study. The main objective of this research is to compare DME with *n*-hexane in terms of the capability of viscosity reduction for Athabasca bitumen. In addition, new experimental data are presented for bubblepoint pressures, densities, and viscosities of Athabasca bitumen and its mixtures with DME and *n*-hexane.

Results show that DME results in slightly higher viscosity than *n*-hexane when they are mixed with the same Athabasca bitumen at a given pressure, temperature, and molar concentration. For example, the equimolar mixture of DME with Athabasca bitumen is 79 cp, and that of *n*-hexane with the same bitumen is 49 cp at 328 K and 60 bar. However, the two solvents are equivalent as diluent at temperatures higher than 380 K. For example, the difference is approximately 1 cp at 382 K and 35 bar between the equimolar mixture of Athabasca bitumen with DME and that with *n*-hexane.

The viscosity data measured for bitumen/*n*-hexane mixtures and bitumen/DME mixtures in this research were correlated with three different viscosity models: a modified Arrhenius model, the power-law model, and the Walther (1931) model. The viscosity data were well-correlated with the modified Arrhenius model, but not with the original Arrhenius (log-linear mixing) rule. The modified Arrhenius model can be used directly with a commercial simulator.

Liquid/liquid separation for solvent/bitumen mixtures, which occurred for *n*-butane/Athabasca bitumen in Gao et al. (2017), was not observed for any of the DME/bitumen and *n*-hexane/bitumen mixtures in this research. The highest solvent concentration in this study was 80 mol% DME for the DME/bitumen system and 92 mol% *n*-hexane for the *n*-hexane/bitumen system.

Introduction

SAGD has been widely used for in-situ recovery of bitumen, which is usually immobile at reservoir conditions. SAGD uses two horizontal wells that are approximately 5 m apart vertically. The upper horizontal well is for injection of high-quality steam (e.g., 90%), and the lower well for production of heated bitumen and water. The injected steam forms a steam-saturated zone or "steam chamber." Bitumen is effectively made mobile by the latent heat of the injected steam upon its condensation near the edge of a steam chamber because the viscosity of bitumen is sensitive to temperature. The main drawback of SAGD is the significant use of energy and water to generate steam.

The energy efficiency of steam-injection processes is quantified by the cumulative steam/oil ratio (CSOR), defined as the ratio of the cumulative volume of steam injected (coldwater equivalent) to the cumulative volume of bitumen produced. In SAGD, temperatures inside the steam chamber and in its vicinity can be high (approximately 450 to 520 K). According to Shen (2013), CSOR is generally in the range from 2 to 4 m^3/m^3 for SAGD to be economically feasible. It is desirable to lower CSOR by operating at low chamber temperatures while maintaining economically sustainable rates of oil production. SAGD is expected to be even less energy-efficient for highly heterogeneous reservoirs (Venkatramani and Okuno 2018). Therefore, there is a critical need to reduce the SAGD CSOR, which has motivated the search for alternative processes.

Coinjection of steam and solvent for SAGD (solvent-SAGD) has been studied and tested as a potential method to improve the drawbacks of SAGD (Leaute and Carey 2002; Gupta et al. 2005; Gupta and Gittins 2006). Solvent-SAGD processes studied in the literature, such as expanding-solvent SAGD (ES-SAGD) and solvent-aided process, use a small amount of solvents (e.g., a few percent to 20% by liquid-volume equivalent) (Leaute and Carey 2002; Gupta et al. 2005; Gupta and Gittins 2006). They aim to enhance the oleic (*L*)-phase mobility by the dilution of oil by solvent, in addition to the thermal energy released from the injected steam. Various researchers have shown that solvent-SAGD has the potential of increasing bitumen-drainage rate and displacement efficiency while reducing CSOR, such as in EnCana's solvent-aided-process pilot (Leaute and Carey 2002; Nasr et al. 2003; Gupta et al. 2005; Gupta and Gittins 2006; Gates 2007; Li et al. 2011a, 2011b; Keshavarz et al. 2014, 2015).

Prior investigations into solvent-SAGD are mainly concerned with hydrocarbon solvents, such as propane (C_3), butane (C_4), and diluents, which usually consist of pentane (C_5) and heavier hydrocarbons at different concentrations (Nasr et al. 2003; Gates 2007; Ivory et al. 2008; Li et al. 2011a, 2011b; Keshavarz et al. 2014, 2015). The suitability of hydrocarbon solvents for SAGD in terms of phase behavior has been reported to increase with increasing carbon number (or decreasing volatility), and tends to level off at a certain carbon number [e.g., approximately *n*-hexane for Athabasca-bitumen reservoirs (Li et al. 2011a; Mohebati et al. 2012; Keshavarz et al. 2015)]. However, heavy hydrocarbon solvents, such as *n*-hexane and diluents, are relatively expensive in general. In-situ retention of the coinjected solvent, which inevitably occurs under heterogeneity, can substantially affect the economics of the project. That is, the geological uncertainties associated with reservoir heterogeneity increase the uncertainty of the economics of the project, if the solvent to be coinjected is expensive.

This paper (SPE 187182) was accepted for presentation at the SPE Annual Technical Conference and Exhibition, San Antonio, Texas, USA, 9–11 October 2017, and revised for publication. Original manuscript received for review 13 September 2017. Revised manuscript received for review 2 June 2018. Paper peer approved 6 June 2018.

The current paper is part of the research motivated by the question of how we can use the water component and/or the aqueous (W) phase to improve the efficiency of steam-based oil recovery such as SAGD and cyclic steam stimulation. This is because water is by far the most-dominant component in steam-based oil recovery for heavy-oil and bitumen recovery (Zhu and Okuno 2016). The volume of produced water is at least a few times greater than the volume of produced oil in SAGD and cyclic steam stimulation.

Sheng et al. (2018) studied a water-soluble solvent, DME, in their phase-behavior analysis and mechanistic simulations of DME-SAGD. Their results showed that DME-SAGD resulted in 35% lower SOR than SAGD, while being able to maintain bitumen-production rates close to those of SAGD. As part of their study, Sheng et al. (2018) compared C_4-SAGD and DME-SAGD, because DME is between C_3 and C_4 in terms of vapor pressure and because C_3-SAGD did not show any improvement over SAGD in their cases as a result of substantially low chamber-edge temperatures. The key hypothesis that can be derived from their mechanistic simulation results is that the solvent's solubility in water makes DME-SAGD substantially different from solvent-SAGD with conventional hydrocarbon solvents through its effect on chamber-edge temperature and compositional distribution in the reservoir. A detailed investigation of how and why they are different might lead to new findings toward an efficient alternative method of bitumen recovery. Relevant results from Sheng et al. (2018) are summarized here.

First, the condensation temperature for a bitumen/solvent/water mixture at a given operating pressure was shown to increase for a water-soluble solvent. It was confirmed in the Sheng et al. (2018) thermodynamic modeling and reservoir simulations that DME-SAGD results in higher chamber-edge temperatures than C_4-SAGD, although DME is more volatile than C_4. The difference in chamber-edge temperature was approximately 30 K at the operating pressure of 35 bar in Sheng et al. (2018).

Second, the in-situ distribution of DME in DME-SAGD was observed to be substantially different from that of C_4 in C_4-SAGD. The solubility of DME in bitumen was nearly one-half that of C_4 at corresponding chamber-edge conditions at the operating pressure of 35 bar. In DME-SAGD simulations, however, approximately 50 mol% of the in-situ DME was used for dilution of bitumen, which was equivalent to the fraction of the in-situ C_4 used for bitumen dilution in C_4-SAGD. This likely occurred because the partitioning of DME into bitumen and water reduced the gravity segregation of the two-liquid-phase flow along the edge of the steam chamber in DME-SAGD. The reduced gravity segregation in DME-SAGD was simulated to facilitate the mixing of condensed DME with bitumen beyond the edge of the steam chamber. This was in contrast to C_4-SAGD, in which the L phase diluted by a substantial amount of C_4 was much less dense than the W phase, impeding the contact between the C_4 bank and bitumen along the edge of the steam chamber.

Third, simulation results showed that the vapor fraction of the in-situ solvent was much smaller in DME-SAGD than in C_4-SAGD. In addition, the injected DME was recovered not only by the L phase, but also by the W phase in DME-SAGD because the solubility of DME in the W phase was properly modeled. Therefore, the recovery factor of solvent was simulated to be approximately 15% higher in DME-SAGD than in C_4-SAGD.

However, the viscosity model used for the L phase containing DME was uncertain in the mechanistic simulation study by Sheng et al. (2018). Therefore, the main objective of this research is to quantify the dilution capability of DME in comparison with that of n-hexane using experimental data for the same Athabasca-bitumen sample. The n-hexane is used for the comparison because it has been reported to be one of the most-effective solvents for solvent-SAGD for Athabasca-bitumen reservoirs.

DME-enhanced waterflooding was studied by Chernetsky et al. (2015), Alkindi et al. (2016), Chahardowli et al. (2016), Groot et al. (2016a, 2016b), Parsons et al. (2016), and te Riele et al. (2016). Laboratory experiments, field studies, and simulation results in these publications showed that the solubility of DME in water could yield efficient propagation in the reservoir, oil swelling, a higher oil recovery, and a higher solvent recovery from the produced water.

For the application of DME to heavy-oil recovery, Haddadnia et al. (2018) studied vapor/liquid-equilibrium data for DME/Athabasca bitumen. They measured solubilities, densities, and viscosities of DME/bitumen mixtures and compared DME with propane and n-butane. They found that values of solubility, density, and viscosity of DME/bitumen mixtures at a given condition lie between those of propane/bitumen and n-butane/bitumen mixtures. The data presented for DME/bitumen mixtures by Haddadnia et al. (2018) are useful, but are not sufficient for the main purpose of this research.

The Materials section and the Apparatus and Experiment Procedure section present the materials and experimental procedure for the phase behavior of DME/bitumen and n-hexane/bitumen mixtures. The Experimental Results and Correlations section provides new data for bubblepoint pressures, densities, and viscosities for DME/bitumen and n-hexane/bitumen mixtures. A modified Arrhenius equation is used to match the new viscosity data. In the Discussions section, the viscosities measured for Athabasca bitumen and n-hexane/bitumen mixtures in this research are compared with relevant data published in the literature. Then, the dilution capabilities of DME and n-hexane are compared in terms of reduction of bitumen viscosity.

Materials

The Athabasca-bitumen sample was provided by an SAGD operator. To reduce the amount of water in the bitumen sample provided, the bitumen sample was dehydrated at 393 K under atmospheric pressure. Then, basic properties of Athabasca bitumen were measured by Exova (Edmonton, Alberta, Canada). The molecular weight (MW) of the bitumen sample was measured to be 532 g/mol by freezing-point depression. Simulated distillation analysis was performed up to 993 K **(Fig. 1).** The density of bitumen at 335 K and atmospheric pressure was measured to be 0.985 g/cm^3. Saturates/asphaltenes/resins/aromatics (SARA) analysis gave the following composition: 24.5 wt% saturates, 36.6 wt% aromatics, 21.1 wt% resins, and 17.8 wt% asphaltenes. The water content of the bitumen was confirmed to be less than 0.1 wt% by *ASTM D4006* (2016).

The purity of DME supplied by Praxair was 99.5%. The n-hexane was supplied by Sigma-Aldrich at a purity higher than 99%.

Apparatus and Experiment Procedure

This section presents the main pieces of equipment and the procedure used for measurement of bubblepoints, densities, and viscosities.

Bubblepoint Measurements. A pressure/volume/temperature (PVT) apparatus was set up to measure bubblepoints of solvent/bitumen mixtures at temperatures between 354 and 394 K. **Fig. 2** presents a schematic for the PVT apparatus. A DBR PVT cell (model DBR-0150-100-200-200-286-155) was installed in an oven (Blue M, model DC-1406F). The confining pressure for the PVT cell was controlled by a Teledyne Isco pump (model 100DX). The PVT-cell temperature was measured (in °C) by a calibrated T-type thermocouple. The accuracy of this thermocouple is ±1 K or ± 1°C. The confining pressure was measured (in psi) by an Ashcroft digital pressure gauge. The accuracy of this pressure gauge is ±2.5 psi or ± 0.17 bar.

Before each measurement, the system was cleaned with hexane and toluene. After cleaning, all lines, valves, and feed accumulators were flushed with dry air. The PVT cell was then evacuated for 6 hours at 353 K. Feed accumulators were prepared to store the solvent

and bitumen that were to be injected into the PVT cell. The amount of feed injection was controlled by the Isco pump. The injection flow rate was set at less than 8 cm^3/h to measure an accurate injection volume. The mass and mole fractions of components were calculated using MW and density data from the National Institute of Standards and Technology (NIST) for *n*-hexane and the literature for DME (Wu et al. 2003, 2004; Ihmels and Lemmon 2007; Wu and Yin 2008).

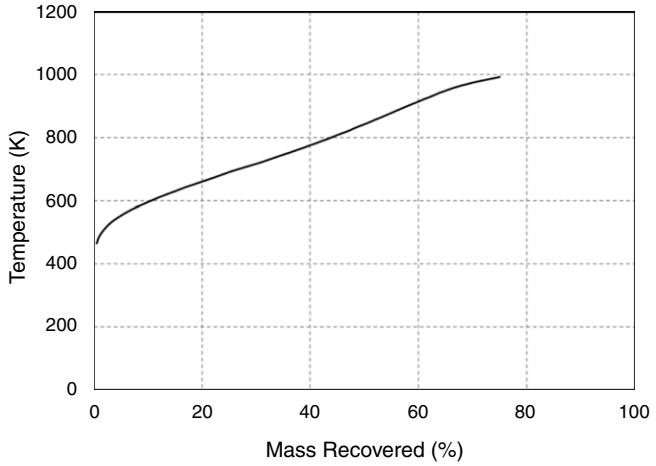

Fig. 1—Simulated distillation results for the Athabasca-bitumen sample studied in this research. The initial boiling point is defined as the temperature corresponding to 0.5% of the total mass recovered. The maximum boiling point reported with this method is 993 K.

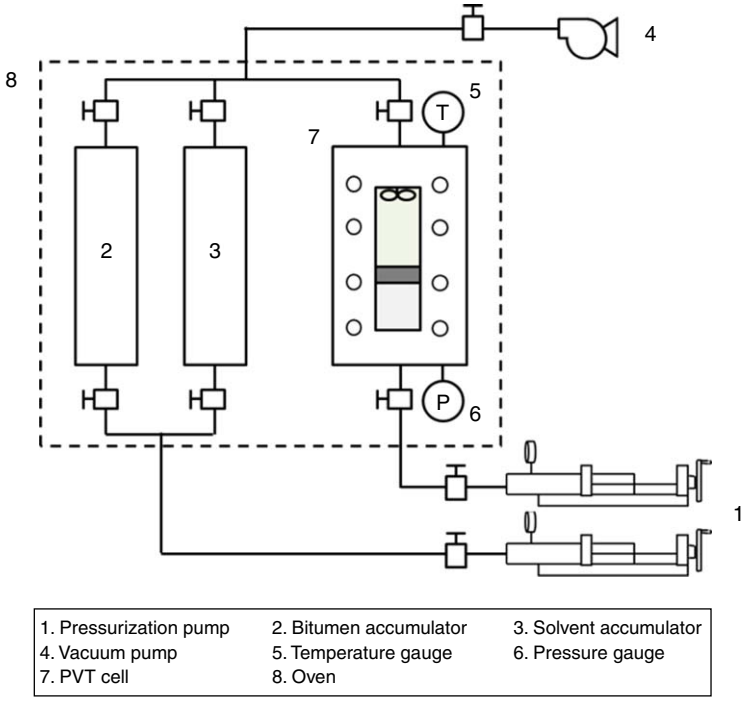

Fig. 2—Schematic of experimental setup for bubblepoint measurement.

For each mixture, the solvent was injected first into the PVT cell. To measure a precise volume, the solvent was injected in the liquid-phase state at room temperature. Because of its high viscosity, bitumen was heated for 1 day and injected into the PVT cell at 333 K. After the injection of solvent and bitumen, the oven was set to a target temperature (354 to 394 K), and the magnetic mixer equipped inside the PVT cell was operated to enhance the mixing of components. The PVT-cell pressure was set sufficiently higher than the vapor pressure of the solvent at the temperature that allows the mixture to be a single-phase liquid. The system was left for at least 1 day while using the magnetic mixer. An equilibrium state of the mixture was confirmed by constant temperature and pressure in the PVT cell and also constant volume in the pump.

Bubblepoints were measured by the constant-mass-expansion method, in which the total fluid volumes were recorded at different pressures. The pressure of the mixture was initialized at a high pressure so that it was a single-phase liquid, and then it was decreased by 1.4 bar/hr. While decreasing the pressure, the mixture was stirred by the magnetic mixer to accelerate the equilibration process at a new pressure. After the PVT-cell pressure reached the next target pressure, the magnetic mixer was turned off. The mixture was then kept in static state for at least 2 hours. This period of time was sufficient for the mixture to reach a single-phase equilibrium state. The pressure was kept constant while the system reached an equilibrium state. Equilibrium was confirmed when the PVT-cell pressure was stable with no volume change. When the mixture formed two equilibrium phases, it took a longer period of time for equilibration. After

a vapor phase appeared, the pressure was decreased by 0.34 to 0.69 bar every 5 hours while the magnetic mixer was on. After the PVT-cell pressure reached the target pressure, the magnetic mixer was turned off, and the mixture was kept in static state for at least 10 hours. Equilibrium was confirmed by a stable pressure in the PVT cell and a constant fluid volume.

After one constant-mass expansion was completed at a given temperature, the PVT cell was pressurized at greater than the vapor pressure of the solvent. Then, a new temperature was set and left for at least 1 day to reach a new equilibrium state. The magnetic mixer was kept on during this time. After reaching a new equilibrium state, the same procedure of constant-mass expansion was repeated to measure a new bubblepoint.

The volume changes and the pressure of the PVT cell were recorded at each expansion step. The volume change was also detected through the visual window with the cathetometer. Three bubblepoint measurements for DME/bitumen mixtures and two bubblepoint measurements for *n*-hexane/bitumen mixtures were performed in this research.

Density and Viscosity Measurements. A schematic of the system for density and viscosity measurements is shown in **Fig. 3.** It consists of automated pumps, a mixing accumulator, an in-line density meter, an in-line viscometer, an oven, a backpressure regulator (BPR), and an accumulator for the effluent. The pump (Teledyne Isco 100DX) pressurizes and maintains the pressure of the system automatically by deionized water. A mixing accumulator was used as an equilibrium cell, where the fluid sample is prepared homogeneously. The capacity of the mixing accumulator is 1290 cm^3.

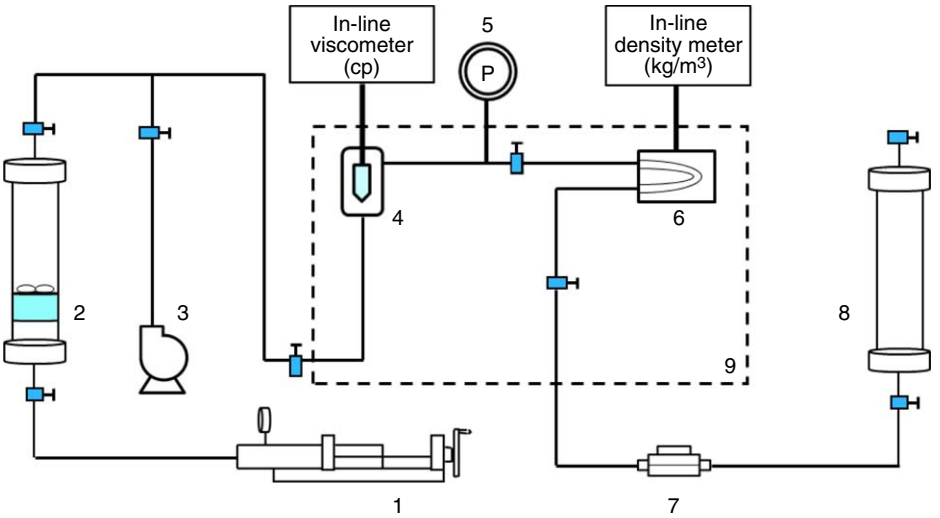

Fig. 3—Schematic of experimental setup for density and viscosity measurement.

In the density-measuring cell (Anton Paar), the density of the fluid is measured in a U-shaped tube in the range from 0 to 3000 kg/m^3. The accuracy of the density meter is ± 1 kg/m^3. The pressure and temperature ranges of the density meter are 0 to 1,400 bar and 263 to 473 K, respectively. For this research, it was calibrated with water and nitrogen for temperatures in the range from 293 to 473 K and pressures from 1.01 to 100 bar. Density values for calibration were taken from NIST. The in-line viscometer (Hydramotion XL7 series) measures the fluid viscosity in the range from 0.1 to 10,000 cp. The pressure limit is 10,000 psi (700 bar), and the temperature limit is 723 K. This is a resonant (or vibrational) viscometer that creates waves within the liquid being measured. The viscosity accuracy is $\pm 1\%$ of the reading, and the repeatability is $\pm 0.3\%$ of the reading.

Both the viscometer and the density meter were installed inside a Despatch oven (model LAC2-18-8). Light-emitting-diode screens that display measured data from the density meter and the viscometer were connected outside the oven. The absolute pressure of the system was measured in bar with a pressure gauge (Omega PX459-2.5KGI-EH) located between the density meter and the viscometer. The pressure of the system was maintained with the BPR installed outside of the oven. The temperature for the density meter was measured (in °C) with an accuracy $\pm$ 0.1°C.

Before each measurement, the system was cleaned thoroughly with toluene and dried with air. Cleaning was complete when the density meter and the viscometer displayed the NIST density and viscosity values for toluene at the specific temperature and pressure conditions. The system was then evacuated for at least 6 hours and filled with helium at 68.6 bar. The pressure was monitored for 1 day to ensure that no leakages occurred for the setup. The total fluid volume of the system was 30 cm^3.

At 296 K and 20.7 bar, mixtures containing bitumen and solvent were prepared at two mixing ratios: 11.6 vol% of solvent and 88.4 vol% of bitumen, and 19.8 vol% of solvent and 80.2 vol% of bitumen. Mixtures were completely stirred for at least 1 day. To start an experiment, the mixture was first injected from the mixing accumulator at 5 cm^3/h and 68.6 bar to remove the helium of the system. Helium was used to prevent the flash vaporization of the mixture inside the system. Once 30 cm^3 of the sample was injected, the flow rate was changed to 50 cm^3/h for a total volume of 60 cm^3. This injection procedure is to remove trapped helium inside the system. The density and viscosity of 100% bitumen, DME/bitumen mixtures, and *n*-hexane/bitumen mixtures were measured from 323 to 443 K and 15 to 70 bar. Measurements were performed at a fixed temperature by increasing pressure within the closed system inside the oven.

Experimental Results and Correlations

Bubblepoints, densities, and viscosities were measured for the bitumen and its mixtures with solvents at a wide range of temperatures and pressures. As summarized in **Table 1,** nine mixtures were studied for the experiments: five DME/bitumen mixtures (DB-1, DB-2,

DB-3, DB-4, and DB-5) and four *n*-hexane/bitumen mixtures (HB-1, HB-2, HB-3, and HB-4). Bubblepoints were measured for DB-1, DB-2, DB-3, HB-1, and HB-2. Densities and viscosities were measured for DB-4, DB-5, HB-3, and HB-4.

Bubblepoint Data. **Table 2** presents the bubblepoints measured for the three DB mixtures and the two HB mixtures. One of the observation points was whether liquid/liquid separation occurs for these mixtures, especially for HB-2, because of its high solvent concentration.

Mixture	DME (mol%)	Bitumen (mol%)	Mixture	*n*-Hexane (mol%)	Bitumen (mol%)
DB-1	80.0	20.0	HB-1	80.0	20.0
DB-2	47.0	53.0	HB-2	92.0	8.0
DB-3	20.0	80.0	HB-3	50.0	50.0
DB-4	65.4	34.6	HB-4	34.6	65.4
DB-5	50.0	50.0			

Table 1—Compositions of the DME/bitumen (DB) and *n*-hexane/bitumen (HB) mixtures studied in this paper.

Mixture	Temperature (K)	Bubblepoint Pressure (bar)	Mixture	Temperature (K)	Bubblepoint Pressure (bar)
DB-1	354	19.6	HB-1	384	3.5
	366	27.2		394	3.8
	394	42.0			
DB-2	354	11.0	HB-2	379	3.6
	365	13.8		394	4.1
	393	19.2			
DB-3	354	5.0			
	366	6.6			
	394	8.5			

Table 2—Experimental results for bubblepoint pressures. For DME/bitumen mixtures, bubblepoints were measured at 354, 366, and 394 K. For *n*-hexane/bitumen mixtures, bubblepoints were measured at 379, 384, and 394 K.

In Gao et al. (2017), a mixture of 97.24 mol% *n*-butane (C_4) and 2.76 mol% Athabasca bitumen exhibited liquid/liquid separation of hydrocarbons for a wide range of temperatures from 323 to 433 K at pressures relevant to solvent-SAGD for Athabasca-bitumen reservoirs. Because such liquid/liquid separation is expected to affect bitumen transport beyond the edge of the steam chamber, Gao et al. (2018) later conducted a phase-behavior study for *n*-hexane/Athabasca-bitumen and *n*-octane (C_8)/Athabasca-bitumen mixtures. They did not observe liquid/liquid separation for these mixtures, even at high solvent concentrations such as 97.53 mol% *n*-hexane and 93.71 mol% *n*-octane, in their mixtures with Athabasca bitumen.

Zou et al. (2007) detected liquid/liquid separation by using X-ray transmission tomography and in-line density measurement. Gao et al. (2017, 2018) applied backlight to observe color differences among different phases for bitumen/solvent mixtures and bitumen/solvent/water mixtures. This was effective for detecting the separation of solvent-rich liquid and bitumen-rich liquid in Gao et al. (2017). Gao et al. (2017, 2018) also used pressure/volume plots to detect phase changes.

Liquid/liquid separation was not observed in the current research. First, no color difference was observed in the liquid phase. Second, pressure/volume plots in this research indicated only the transition from a single liquid (*L*) to two-phase vapor/liquid (*V*/*L*). Note that the bitumen sample in the current research is different from the one used in Gao et al. (2017, 2018). For example, the MW of the Athabasca-bitumen sample in Gao et al. (2017, 2018), 635 g/mol, is approximately 19% higher than that of the Athabasca-bitumen sample used in this research.

Results indicate that bubblepoint pressures of HB-1 at 384 K and HB-2 at 379 K were measured at higher than the vapor pressures of 100% *n*-hexane at the corresponding temperatures taken from NIST. Gao et al. (2018) also observed that bubblepoint pressures for *n*-hexane/bitumen mixtures were higher than for 100% *n*-hexane for their Athabasca-bitumen sample, for which the water content was measured to be 0.245 wt% by Exova.

Density and Viscosity Data. Densities of the Athabasca bitumen were measured at temperatures from 316 to 451 K and pressures from 1.6 to 100 bar (see **Table 3** and **Fig. 4**). Fig. 4 shows that bitumen density decreases with increasing temperature and with decreasing pressure. For example, the density of bitumen at 28 bar was approximately 997 kg/m^3 at 316 K, but decreased to approximately 913 kg/m^3 at 451 K. Viscosities of the same bitumen were measured at temperatures from 328 to 443 K and pressures from 1.7 to 100 bar (see **Table 4** and **Fig. 5**). As expected, the bitumen viscosity is sensitive to temperature. The bitumen viscosity at 28 bar was measured to decrease from approximately 2,479 cp at 328 K to 3.5 cp at 443 K.

For bitumen mixtures with DME and *n*-hexane, density and viscosity measurements were conducted for DB-4, DB-5, HB-3, and HB-4 (Table 1). The solvent/bitumen mixing ratio was set to be 14 wt% solvent and 86 wt% bitumen for DB-4 and HB-3, and 8 wt% solvent and 92 wt% bitumen for DB-5 and HB-4. With these four mixtures, comparison of measured viscosities for DME and *n*-hexane can be made at the same mixing ratios in mole and weight (i.e., DB-5 and HB-3 at 50 mol% dilution, DB-4 and HB-3 at 14 wt% dilution, and DB-5 and HB-4 at 8 wt% dilution). The measured densities and viscosities are tabulated as follows: **Table 5** for DB-4, **Table 6** for DB-5, **Table 7** for HB-3, and **Table 8** for HB-4.

Temperature: 316 K		Temperature: 329 K		Temperature: 353 K	
Pressure (bar)	Density (kg/m^3)	Pressure (bar)	Density (kg/m^3)	Pressure (bar)	Density (kg/m^3)
1.6	995	1.9	987	1.8	972
3.5	996	2.0	987	13.8	972
6.9	996	3.6	987	27.7	973
10.3	996	6.9	988	41.3	974
13.8	996	10.3	988	55.2	975
17.3	996	13.7	988	69.0	976
20.7	996	17.2	988	82.9	977
24.1	997	20.7	988	100.1	978
27.6	997	24.2	988	–	–
27.6	997	27.6	989	–	–
31.0	997	31.1	989	–	–
34.4	997	34.5	989	–	–
38.0	997	41.3	989	–	–
41.3	998	48.3	990	–	–
44.9	998	55.3	990	–	–
48.3	998	62.2	991	–	–
51.7	998	69.0	991	–	–
55.1	998	75.9	991	–	–
58.6	998	82.8	992	–	–
62.1	999	89.7	992	–	–
65.5	999	96.6	992	–	–
69.0	999	100.0	992	–	–
72.4	999	–	–	–	–
75.9	999	–	–	–	–
79.3	999	–	–	–	–
82.7	1000	–	–	–	–
86.2	1000	–	–	–	–
89.6	1000	–	–	–	–
93.1	1000	–	–	–	–
96.6	1000	–	–	–	–
100.0	1000	–	–	–	–
Temperature: 384 K		Temperature: 419 K		Temperature: 451 K	
Pressure (bar)	Density (kg/m^3)	Pressure (bar)	Density (kg/m^3)	Pressure (bar)	Density (kg/m^3)
1.7	953	1.7	931	1.7	910
13.8	954	13.8	932	13.8	912
27.7	955	27.7	933	27.6	913
41.4	956	41.4	934	41.4	914
55.2	957	55.3	935	55.2	916
69.0	958	69.1	936	69.0	917
82.8	959	83.1	937	82.8	918
100.1	960	100.0	938	100.1	919

Table 3—Experimental results for the bitumen density. Densities were measured at the temperature range from 316 to 451 K and the pressure range from 1.6 to 100 bar.

At the equimolar condition (50 mol% solvent and 50 mol% bitumen), the viscosity of *n*-hexane/bitumen was lower than that of DME/bitumen at the same pressure and temperature. However, the viscosity of the two mixtures became closer at higher temperatures. For example, comparison of DB-5 and HB-3 at 60 bar (Tables 6 and 7) indicates that the viscosity of DME/bitumen was 30 cp higher at 328 K, but only 1.2 cp higher at 382 K **(Fig. 6).** A detailed analysis of the viscosities measured for the bitumen and solvent/bitumen mixtures is presented in the Discussion section after introducing correlations for densities and viscosities in the Correlations for Density and Viscosity of Solvent/Bitumen Mixtures subsection.

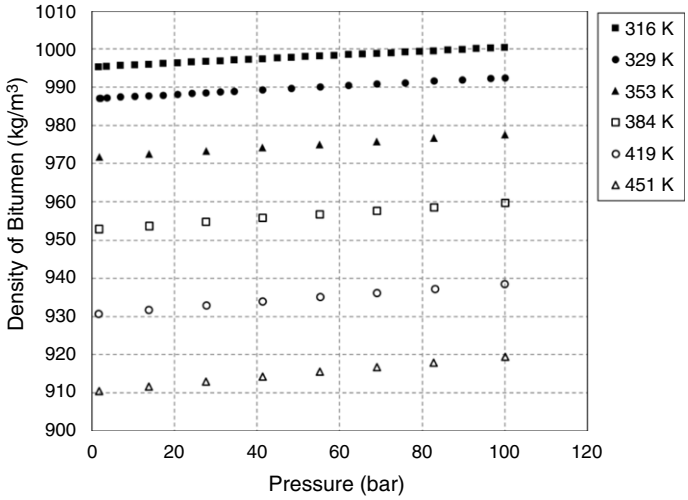

Fig. 4—Experimental results for the bitumen density. Densities were measured at the temperature range from 316 to 451 K and the pressure range from 1.6 to 100 bar. Each data point is summarized in Table 3.

Temperature: 328 K		Temperature: 352 K		Temperature: 380 K	
Pressure (bar)	Viscosity (cp)	Pressure (bar)	Viscosity (cp)	Pressure (bar)	Viscosity (cp)
1.7	2290	1.8	271	1.7	44.4
13.8	2380	13.8	286	13.9	45.9
27.7	2470	27.7	293	27.7	47.6
41.4	2580	41.3	305	41.4	49.5
55.2	2690	55.2	317	55.9	51.3
70.0	2810	69.0	330	69.0	53.2
82.9	2940	82.9	344	82.8	55.2
100.0	3110	100.1	362	100.1	57.7
Temperature: 413 K		Temperature: 443 K			
Pressure (bar)	Viscosity (cp)	Pressure (bar)	Viscosity (cp)		
1.7	9.3	1.7	3.3		
13.8	9.6	13.8	3.4		
27.7	9.9	27.6	3.5		
41.4	10.2	41.4	3.5		
55.3	10.6	55.2	3.7		
69.1	11.0	69.0	3.8		
82.9	11.3	82.8	3.9		
100.0	11.8	100.1	4.0		

Table 4—Experimental results for the bitumen viscosity. Viscosities were measured at the temperature range from 328 to 443 K and the pressure range from 1.6 to 100 bar.

Correlations for Density and Viscosity of Solvent/Bitumen Mixtures. The density data measured for the bitumen in this research have been correlated with the equation used by Nourozieh et al. (2015a),

$$\rho_{bit} = \rho_0 \exp(\alpha P), \quad \ldots\ldots (1)$$

$$\rho_0 = a_1 + a_2 T + a_3 T^2, \quad \ldots\ldots (2)$$

$$\alpha = a_4 \exp(a_5 T), \quad \ldots\ldots (3)$$

where ρ_{bit} is bitumen density (in kg/m^3), P is pressure (in MPa), and T is temperature (in °C). The five parameters a_1 through a_5 are adjusted to match the experimental data in this research. The resulting average absolute deviation (AAD) and average absolute relative deviation (AARD) are 0.75 kg/m^3 and 0.08%, respectively, with $a_1 = 1022.11$, $a_2 = -0.61$, $a_3 = 0$, $a_4 = 3.53 \times 10^{-4}$, and $a_5 = 3.30 \times 10^{-4}$.

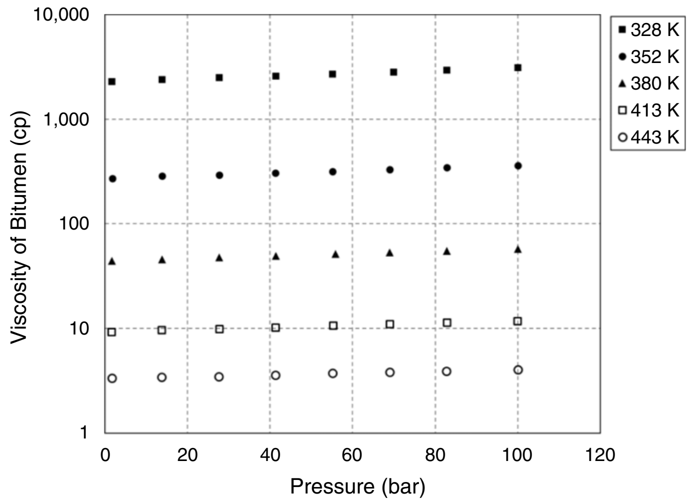

Fig. 5—Experimental results for the bitumen viscosity. Viscosities were measured at the temperature range from 328 to 443 K and the pressure range from 1.6 to 100 bar. Each data point is summarized in Table 4.

Density			Viscosity		
Temperature (K)	Pressure (bar)	Density (kg/m^3)	Temperature (K)	Pressure (bar)	Viscosity (cp)
328	30.0	927	327	30.0	17.2
	35.0	927		35.0	19.7
	40.0	928		40.0	21.1
	50.0	928		50.0	22.4
	60.0	929		60.0	23.6
	70.0	930		70.0	24.6
355	30.0	906	354	30.0	4.7
	35.0	907		35.0	5.3
	40.0	907		40.0	5.8
	50.0	908		50.0	6.3
	60.1	909		60.1	6.7
	70.0	910		70.0	7.0
384	35.0	884	380	35.0	1.9
	40.0	885		40.0	2.1
	50.0	886		50.0	2.3
	60.0	887		60.0	2.5
	70.0	888		70.0	2.6
418	50.0	860	414	50.0	1.0
	60.0	861		60.0	1.1
	70.0	862		70.0	1.2

Table 5—Experimental results for the density and viscosity of DB-4. DB-4 consists of 65.4 mol% DME and 34.6 mol% bitumen, or 14 wt% DME and 86 wt% bitumen.

The viscosity data measured for the bitumen in this research are correlated using the correlation of Mehrotra and Svrcek (1986),

$$\ln(\mu_{\text{bit}}) = \exp[b_1 + b_2 \ln(T + 273.15)] + b_3 P_g, \quad (4)$$

where T is temperature (in °C) and P_g is gauge pressure (in MPa). The resulting AAD and AARD are 32.7 cp and 18.3%, respectively, with $b_1 = 33.33463$, $b_2 = -5.40032$, and $b_3 = 0.023782$.

Wu et al. (2003) presented the following correlation for saturated-liquid DME,

$$\log_{10}\mu_{DME} = -5.7282 + \frac{631.031}{T} + 0.01453T - 1.8225 \times 10^{-5}T^2, \quad (5)$$

where μ is the DME viscosity (in cp) and T is temperature (in K). This correlation gave 0.5% AARD from experimental data measured from 227 to 343 K. Viscosities of *n*-hexane are taken from NIST, in which the *n*-hexane viscosities are calculated using the correlation presented in Michailidou et al. (2013). In terms of solvent viscosity, DME is less viscous than *n*-hexane. For example, the viscosities of DME and *n*-hexane at 35 bar are compared in **Fig. 7.**

Density			Viscosity		
Temperature (K)	Pressure (bar)	Density (kg/m^3)	Temperature (K)	Pressure (bar)	Viscosity (cp)
328	20.1	948	328	20.1	38.2
	25.0	948		25.0	36.7
	35.1	949		35.1	36.7
	40.0	949		40.0	48.1
	50.0	950		60.0	79.0
	60.0	950		70.1	87.5
	70.1	951		–	–
355	30.0	930	355	30.0	10.9
	35.0	930		35.0	10.4
	40.0	931		40.0	11.2
	50.0	931		50.0	14.2
	60.0	932		60.0	17.8
	70.1	933		70.1	21.2
384	30.1	909	382	30.1	3.8
	35.0	909		35.0	3.7
	40.0	910		40.0	3.5
	50.0	911		50.0	5.5
	60.0	911		60.0	4.7
	70.0	912		70.1	5.6
417	40.0	886	414	40.0	1.9
	50.0	887		50.0	1.9
	60.1	888		60.1	1.6
	70.0	889		70.0	1.9
446	50.1	865	443	50.0	1.6
	60.0	867		70.0	0.9
	70.0	868		–	–

Table 6—Experimental results for the density and viscosity of DB-5. DB-5 consists of 50 mol% DME and 50 mol% bitumen, or 8 wt% DME and 92 wt% bitumen.

Density			Viscosity		
Temperature (K)	Pressure (bar)	Density (kg/m^3)	Temperature (K)	Pressure (bar)	Viscosity (cp)
328	15.0	919	327	15.0	22.4
	35.0	921		35.0	30.6
	60.0	922		60.0	49.0
354	15.0	902	353	15.0	6.0
	35.0	903		35.0	7.4
	60.0	905		60.0	11.8
383	15.0	882	382	15.0	2.4
	35.0	883		35.0	2.5
	60.0	885		60.0	3.5
417	15.0	858	414	15.0	1.2
	35.0	860		35.0	1.2
	60.0	863		60.0	1.3
446	15.1	838	443	15.0	1.0
	35.0	840		35.0	1.0
	60.0	843		60.0	0.7

Table 7—Experimental results for the density and viscosity of HB-3. HB-3 consists of 50 mol% *n*-hexane and 50 mol% bitumen, or 14 wt% *n*-hexane and 86 wt% bitumen.

Density			Viscosity		
Temperature (K)	Pressure (bar)	Density (kg/m^3)	Temperature (K)	Pressure (bar)	Viscosity (cp)
	14.7	948		15.0	80.5
328	35.0	949	327	35.0	223
	60.0	951		60.0	246
	15.0	930		15.0	14.0
355	35.0	931	354	35.0	31.1
	60.1	933		60.0	45.2
	15.0	911		15.0	4.0
384	35.0	913	382	35.0	7.0
	60.1	914		60.0	11.1
	15.0	888		15.0	1.6
418	35.0	890	414	35.0	1.9
	60.0	893		60.0	3.2
	15.0	868		15.0	1.1
447	35.0	871	443	60.2	1.4
	60.2	873		–	–

Table 8—Experimental results for the density and viscosity of HB-4. HB-4 consists of 34.6 mol% *n*-hexane and 65.4 mol% bitumen, or 8 wt% *n*-hexane and 92 wt% bitumen.

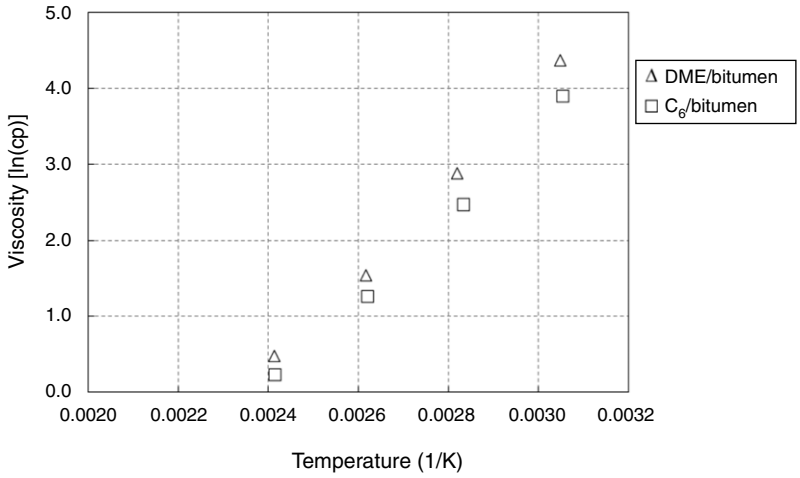

Fig. 6—Experimental results for the equimolar mixture of solvent and bitumen, DB-5 and HB-3, at 60 bar. The viscosity of the DME/bitumen and *n*-hexane (C_6)/bitumen mixtures becomes similar with increasing temperature. See Tables 6 and 7 for the viscosity data.

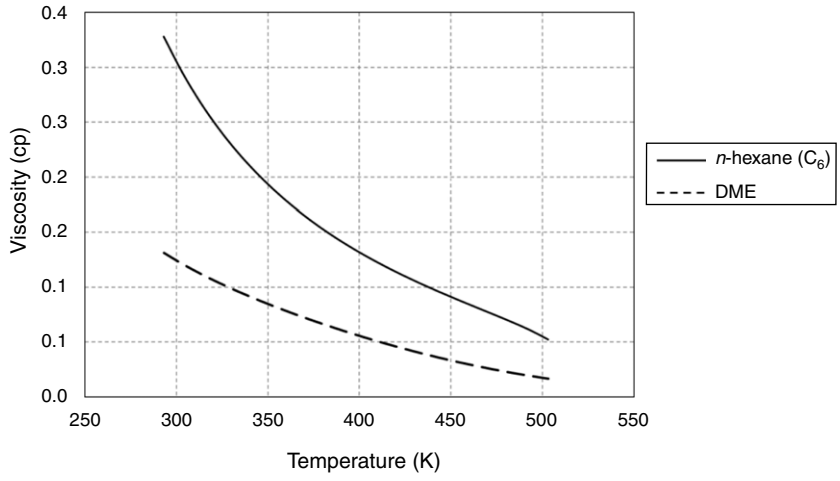

Fig. 7—Viscosity of DME and *n*-hexane (C_6) at 35 bar. DME viscosity was calculated by Eq. 5 (Wu et al. 2003). The *n*-hexane viscosity was taken from NIST. This clearly shows that DME is less viscous than *n*-hexane.

The viscosity data for the two mixtures, DME/bitumen and *n*-hexane/bitumen, are correlated with the following three models: a modified Arrhenius model, the power-law model, and the Walther (1931) model. The modified Arrhenius equation is used because it is implemented in a commercial reservoir simulator, CMG-STARS (CMG 2014). Therefore, the calibrated model can be directly used to perform numerical simulation of steam/DME coinjection.

The original Arrhenius (1887) equation dependent on kinetic theory is

$$\ln \mu_{\text{mix}} = \sum_{i=1}^{Nc} x_i \ln \mu_i, \quad \ldots\ldots (6)$$

where μ_{mix} is the viscosity of a mixture, μ_i is the viscosity of component i, and x_i is the mole fraction of component i. The modified Arrhenius model used in this research is

$$\ln \mu_L = \sum_{i=1}^{Nc} q_i x_{iL} \ln \mu_{iL}, \quad \ldots\ldots (7)$$

subject to

$$\sum_{i=1}^{Nc} q_i x_{iL} = 1.0, \quad \ldots\ldots (8)$$

where μ_{iL} and x_{iL} are the viscosity and mole fraction of component i in the L phase, respectively, and q_i is the weighting factor for component i. The weighting factors for components except for bitumen are set to be equal, subject to Eq. 8.

For mixtures of bitumen/solvent/water, Venkatramani and Okuno (2017) used the following equation for the weighting factor q_{CD} for the dead-bitumen component (C_D),

$$q_{CD} = 1 + \alpha \left\{ \frac{(1 - x_{CDL})[1 - (1 - x_{CDL})^8]}{x_{CDL}} \right\}, \quad \ldots\ldots (9)$$

where α is a constant specific to the solvent in the mixture of interest. Venkatramani and Okuno (2017) used this equation to account for the difference between the two binaries, bitumen/water and bitumen/solvent, in terms of the viscosity mixing rules presented by Glandt and Chapman (1995). In this research, the α-parameters for DME and *n*-hexane have been determined by matching the viscosity data as follows: 0.291 for DME and 0.0381 for *n*-hexane.

The α-parameter tends to increase from zero as the solvent mixed with bitumen becomes lighter according to the optimized α-values by Venkatramani and Okuno (2017) derived from published data for bitumen/solvent mixtures. The modified Arrhenius equation (Eq. 7) reduces to the original Arrhenius equation (Eq. 6), which is the log-linear mixing rule, when α is set to zero ($q_i = 1.0$ for all i).

Fig. 8 compares the viscosities calculated for DB-5 and HB-3 at 60 bar using Eqs. 6 and 7 with the corresponding experimental data. The original Arrhenius equation reasonably correlates the data for HB-3 (Fig. 8a). With the small value of α, 0.0381, optimized for *n*-hexane/bitumen mixtures, the modified Arrhenius equation is only slightly more accurate. However, Fig. 8b clearly shows that accurate representation of the DB-5 data requires the modified Arrhenius equation.

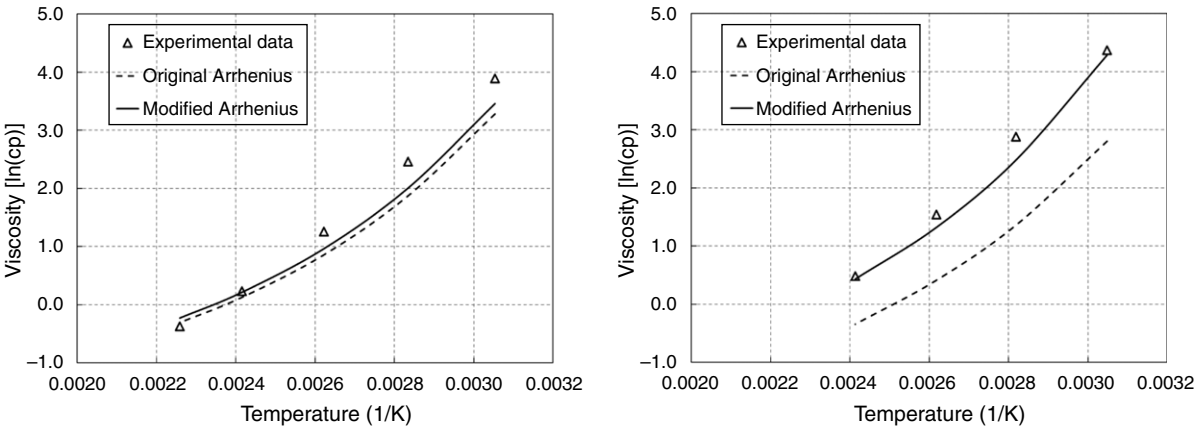

(a) *n*-hexane (C_6) 50 mol%/bitumen 50 mol% (HB-3) at 60 bar (b) DME 50 mol%/bitumen 50 mol% (DB-5) at 60 bar

Fig. 8—Correlations derived from the original and modified Arrhenius equations are compared with the experimental data (50 mol% solvent/50 mol% bitumen) at 60 bar. The original Arrhenius equation shows good agreement with the *n*-hexane (C_6)/bitumen mixture, but it is inaccurate for the DME/bitumen mixture. The modified Arrhenius equation is in good agreement with both mixtures.

In addition to the modified Arrhenius model, the power-law model and the Walther (1931) model are applied to correlate the viscosity data obtained. The power-law model is

$$\mu_{\text{mix}} = [x_s \mu_s^n + (1 - x_s)\mu_{\text{bit}}^n]^{1/n}, \quad \ldots\ldots (10)$$

where μ_s and μ_{bit} are the viscosities of solvent and bitumen, respectively, and x_s is the solvent mole fraction in the mixture. The *n*-parameter was determined to be 0.1416 for bitumen/DME mixtures and 0.0175 for bitumen/*n*-hexane mixtures.

The Walther (1931) model is

$$\ln[\ln(\mu_{\text{mix}}) + C] = v_s \ln[\ln(\mu_s + C)] + (1 - v_s)\ln[\ln(\mu_{\text{bit}} + C)], \quad \ldots\ldots (11)$$

where v_s is the solvent volume fraction in the mixture. The C-parameter was determined to be 0.9641 for bitumen/DME mixtures and 0.9128 for bitumen/*n*-hexane mixtures.

Fig. 9 compares the three viscosity models with the experimental data for DB-5 and HB-3 at 60 bar. It is observed that the Walther (1931) model provides higher values than the other two models, and it therefore provides more-accurate correlation at high-viscosity regions. For the *n*-hexane/bitumen mixtures, all correlations are in reasonable agreement with the experimental data. The modified Arrhenius model and power-law model are similar in correlative accuracy for the *n*-hexane/bitumen mixtures. For the DME/bitumen mixtures, the Walther (1931) model is more accurate at high-viscosity values, but the modified Arrhenius model is more accurate at low-viscosity values.

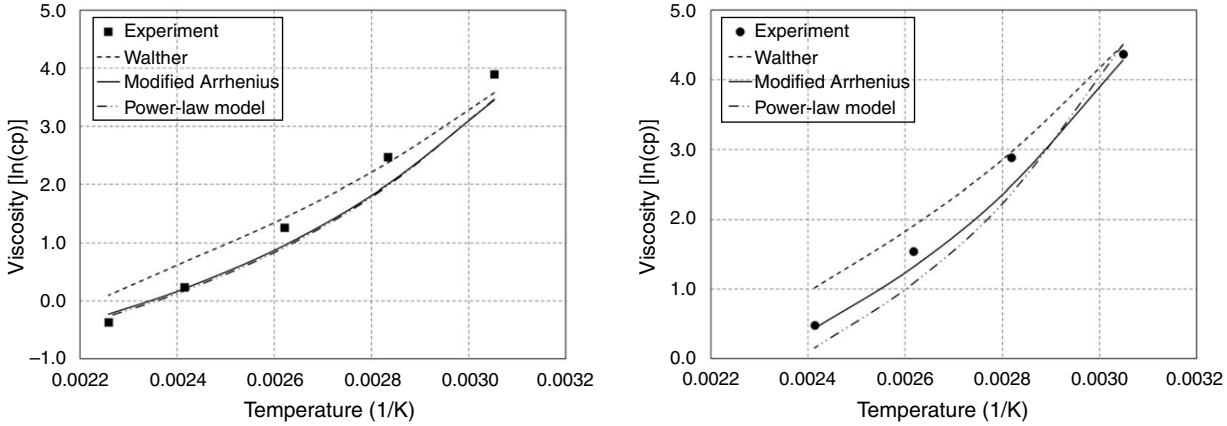

(a) *n*-hexane (C_6) 50 mol%/bitumen 50 mol% (HB-3) at 60 bar

(b) DME 50 mol%/bitumen 50 mol% (DB-5) at 60 bar

Fig. 9—Correlations derived from the modified Arrhenius equation, the power-law equation, and the Walther (1931) equation are compared with the experimental data (50 mol% solvent/50 mol% bitumen) at 60 bar. For the *n*-hexane/bitumen mixture, all correlations are in reasonable agreement with the data. For the DME/bitumen mixture, the Walther (1931) model matches high-viscosity values well, but the modified Arrhenius model matches low-viscosity values well.

For all viscosity data measured for HB-3 and HB-4, the modified Arrhenius equation provides an AAD of 11.9 cp and an AARD of 25.4%. The power-law model provides an AAD of 11.2 cp and an AARD of 26.6%. The Walther (1931) model provides an AAD of 10.6 cp and an AARD of 42.7%. For the DB-4 and DB-5 data, the modified Arrhenius equation provides an AAD of 4.2 cp and an AARD of 22.5%. The power-law model provides an AAD of 6.1 cp and an AARD of 39.6%. The Walther (1931) model provides an AAD of 6.2 cp and an AARD of 40.2%.

Discussion

This section consists of two subsections. In the first subsection, the viscosity data measured for the bitumen and HB-3 and HB-4 are analyzed and compared with the data reported by Nourozieh et al. (2015b) for another Athabasca-bitumen sample and its mixtures with *n*-hexane. In the second subsection, *n*-hexane and DME are compared in terms of viscosity reduction of the oleic (L) phase by dilution, for which the modified Arrhenius equation calibrated with the new data is used.

Viscosity Data for Bitumen and *n*-Hexane/Bitumen. Nourozieh et al. (2015b) measured viscosities of *n*-hexane/Athabasca-bitumen mixtures. The Athabasca-bitumen sample used by Nourozieh et al. (2015a, 2015b, 2015c) was provided by ConocoPhillips. The MW was reported to be 539.2 g/mol, which is close to the MW of 532 g/mol measured for the Athabasca-bitumen sample used in this research (both results were obtained by use of benzene as the solvent). However, the SARA composition of their bitumen sample is markedly different from that of the bitumen used in this research, as shown in **Table 9.** The Athabasca-bitumen sample in this research is richer in saturates than that used in Nourozieh (2015a, 2015b, 2015c). Table 9 also shows the coefficients for Eq. 4 for the two Athabasca-bitumen samples.

		Bitumen (This Research)	Bitumen (Nourozieh et al. 2015a, 2015b, 2015c)
MW (g/mol)		532	539.2
SARA (wt%)	Saturates	24.5	12.26
	Aromatics	36.6	40.08
	Resins	21.1	36.53
	Asphaltenes	17.8 (pentane-insoluble)	11.13 (heptane-insoluble)
Bitumen-viscosity model (Mehrotra and Svrcek 1986)	b_1	33.33463	26.65193
	b_2	–5.40032	–4.04208
	b_3	0.023782	0.031101

Table 9—Properties of bitumen in this research and bitumen used in Nourozieh et al. (2015a, 2015b, 2015c). The two bitumen samples are similar in terms of MW, but markedly different in terms of the saturate concentration. The viscosity model developed by Mehrotra and Svrcek (1986) shows good agreement with both bitumens with different values for parameters b_1, b_2, and b_3. Note that the asphaltene was pentane-insoluble in this research, but heptane-insoluble in Nourozieh et al. (2015a, 2015b, 2015c).

Fig. 10 clearly shows that the bitumen studied in this research is less viscous at all temperatures than the bitumen studied by Nourozieh et al. (2015a, 2015b, 2015c). This viscosity difference can be explained by the difference in the SARA composition (Table 9). Malkin et al. (2016) analyzed the effect of SARA on the viscosity of nearly 200 crude-oil samples. They observed that saturates tend to decrease the oil viscosity, but asphaltenes, resins, and aromatics tend to increase it. The concentration of saturates is twice as high in the bitumen in this research as it is in the bitumen used in Nourozieh et al. (2015a, 2015b, 2015c) (24.5 wt% in comparison with 12.26 wt%). This clear difference in SARA is likely the main reason for the observed difference in Fig. 10. Note that different solvents were used to measure the asphaltene content for the bitumen in this research and the bitumen studied by Nourozieh et al. (2015a, 2015b, 2015c). The asphaltene was pentane-insoluble in this research, but heptane-insoluble in Nourozieh et al. (2015a, 2015b, 2015c).

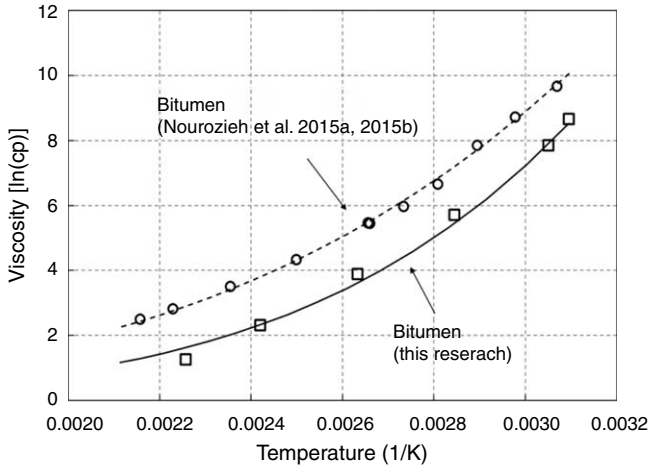

Fig. 10—Viscosity for bitumen in this research and bitumen from Nourozieh et al. (2015a, 2015b). Open circles are experimental data for the bitumen viscosity taken from Nourozieh et al. (2015a, 2015b) at 40 bar. Open squares are experimental data in this research for the bitumen viscosity at 40 bar. The dashed line is the Mehrotra and Svrcek (1986) correlation (Eq. 4) for the bitumen of Nourozieh et al. (2015a, 2015b). The continuous line is the Mehrotra and Svrcek (1986) correlation (Eq. 4) for the bitumen studied in this research. The parameters of the Mehrotra and Svrcek (1986) correlation for two bitumens are tabulated in Table 9.

To validate the experimental viscosity data for the HB-3 and HB-4 mixtures, the power-law model (Eq. 10) with the *n*-parameter from Nourozieh et al. (2015b) is applied. The *n*-parameter was determined to be 0.0186 for the mixtures of *n*-hexane with Athabasca bitumen in Nourozieh et al. (2015b). **Fig. 11a** shows that the viscosities for HB-3 are correlated with the power-law correlation given in Nourozieh et al. (2015b), although the bitumens studied by them and in this research are different from each other (Table 9).

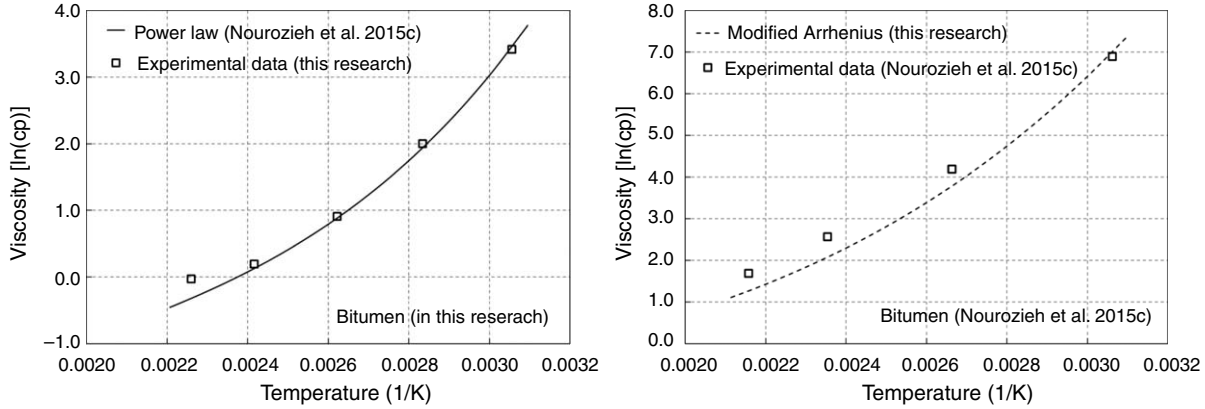

(a) Bitumen (in this research): 50 mol% *n*-hexane (C_6)/50 mol% bitumen (HB-3) at 35 bars

(b) Bitumen (Nourozieh et al. 2015c): 24.8 mol% *n*-hexane (C_6)/75.2 mol% bitumen at 41 bars

Fig. 11—Cross-check of the power-law model and the modified Arrhenius model to correlate experimental data. The parameter (*n*) of the power-law model is 0.0186 from Nourozieh et al. (2015c) and the parameter (α) of the modified Arrhenius model is 0.0381 from this research. It is found that the power-law model from Nourozieh et al. (2015c) fits well with the experimental data in this research. The modified Arrhenius model developed in this research is in good agreement with the experimental data of Nourozieh et al. (2015c), with no change of parameter values. (a) Bitumen (in this research): 50 mol% *n*-hexane (C_6)/50 mol% bitumen (HB-3) at 35 bar; (b) bitumen (Nourozieh et al. 2015c): 24.8 mol% *n*-hexane (C_6)/75.2 mol% bitumen at 41 bar.

In addition, the modified Arrhenius model with $\alpha = 0.0381$ is applied to the experimental data of Nourozieh et al. (2015b). Fig. 11b shows that the modified Arrhenius model (Eq. 7) correlates well the viscosity values for the mixtures of *n*-hexane/Athabasca bitumen measured by Nourozieh et al. (2015b). This indicates that the mixing behavior of the current bitumen sample with *n*-hexane is similar to that of the Nourozieh et al. (2015b) bitumen sample with *n*-hexane.

Dilution Capability of DME and *n*-Hexane. The dilution capabilities of DME and *n*-hexane are compared in terms of oleic (*L*) -phase viscosity using the modified Arrhenius equation calibrated with the new data. The comparison is made for the temperature range from 323 to 473 K, which is deemed relevant to in-situ conditions for the *L*-phase flow in SAGD and solvent-SAGD.

Fig. 12 shows the *L*-phase viscosities calculated for the bitumen and the equimolar mixtures of *n*-hexane/bitumen and DME/bitumen at 35 bar. Overall, DME/bitumen and *n*-hexane/bitumen exhibit similar viscosities. The viscosity of the DME/bitumen mixture is approximately 66 cp higher than that of the *n*-hexane/bitumen mixture at 323 K. However, the difference is calculated to be less than 1 cp at temperatures greater than 383 K. This trend is calculated also at different pressures.

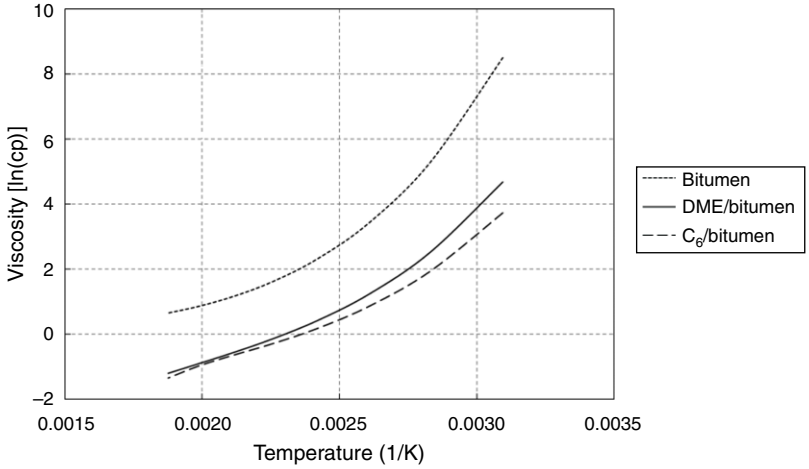

Fig. 12—The viscosity comparison for bitumen, the equimolar mixtures of bitumen with DME, and bitumen with *n*-hexane (C_6) at 35 bar. The viscosities were calculated using the modified Arrhenius model developed in this research.

Fig. 13 shows the *L*-phase viscosities calculated at 35 bar for 100% bitumen, and *n*-hexane/bitumen and DME/bitumen mixtures with two different solvent concentrations, 30 and 70 mol%. Again, the overall effect of DME on bitumen dilution is close to that of *n*-hexane.

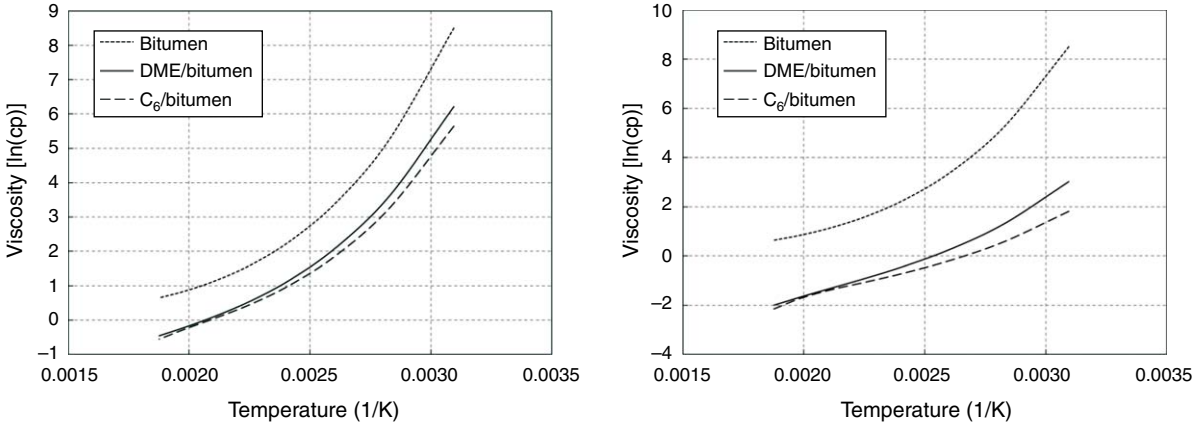

Fig. 13—The viscosity comparison for DME/bitumen, *n*-hexane (C_6)/bitumen, and bitumen at 35 bar with different concentrations of solvent: 30 and 70 mol%. The viscosities were calculated using the modified Arrhenius model developed in this research. (a) 30 mol% solvent/70 mol% bitumen at 35 bar; (b) 70 mol% solvent/30 mol% bitumen at 35 bar.

The experimental results and viscosity correlations indicate that the *n*-hexane/bitumen mixtures provide lower *L*-phase viscosities than the DME/bitumen mixtures, and that they become similar with increasing temperature. This indicates that the viscosity of a less-viscous solvent with bitumen does not necessarily result in lower viscosity than that of bitumen mixtures with a more-viscous solvent at the same concentration. This trend can be also found in the experimental data by Nourozieh et al. (2013), Kariznovi et al. (2013), and Ramos-Pallares et al. (2015).

Ramos-Pallares et al. (2015) measured the viscosity of a bitumen sample from western Canada mixed with a series of *n*-alkanes: ethane, propane, butane, pentane, and heptane. Because their experimental data were given using mass fractions, the concentrations of solvent were converted into the mole fractions with the assumed MW of 500 g/mol for their bitumen sample. It was found that, under the same mole fraction of solvent, the heptane/bitumen mixture was less viscous than the mixtures of the bitumen with ethane and propane, as presented in **Fig. 14a.** Furthermore, a similar observation can be derived from the power-law models made by Nourozieh et al. (2013) and Kariznovi et al. (2013) for *n*-decane and *n*-tetradecane, respectively. That is, the viscosity of *n*-tetradecane/bitumen is calculated to be slightly lower than that of *n*-decane/bitumen, as presented in Fig. 14b.

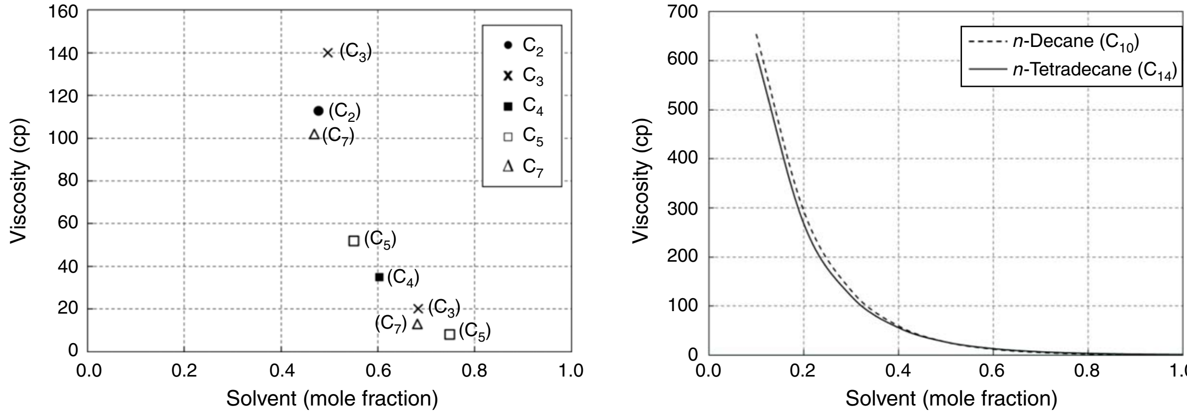

(a) Experimental data for the viscosity of bitumen with different solvents at 373 K (Ramos-Pallares et al. 2015). At the same molar concentration of solvent, *n*-heptane (C_7) gives lower viscosity than ethane (C_2) or propane (C_3) when it is mixed with the same bitumen (western Canada).

(b) The viscosities calculated for *n*-decane (C_{10}) and *n*-tetradecane (C_{14}) with Athabasca bitumen at 343 K and 40 bars by the power law model of Nourozieh et al. (2013) and Kariznovi et al. (2013). *n*-Tetradecane (C_{14}) gives lower viscosity than *n*-decane (C_{10}) when mixed with Athabasca bitumen.

Fig. 14—Experimental data and viscosity correlations show that bitumen mixed with a heavier solvent results in lower viscosity than that with a lighter solvent. (a) Experimental data for the viscosity of bitumen with different solvents at 373 K (Ramos-Pallares et al. 2015). At the same molar concentration of solvent, *n*-heptane (C_7) provides lower viscosity than ethane (C_2) or propane (C_3) when it is mixed with the same bitumen (western Canada). (b) The viscosities calculated for *n*-decane (C_{10}) and *n*-tetradecane (C_{14}) with Athabasca bitumen at 343 K and 40 bar using the power-law model of Nourozieh et al. (2013) and Kariznovi et al. (2013). The *n*-tetradecane (C_{14}) provides lower viscosity than *n*-decane (C_{10}) when mixed with Athabasca bitumen.

To further investigate the dilution capability of DME compared with *n*-alkane solvents, the modified Arrhenius equation has been calibrated with the viscosity data measured by Nourozieh et al. (2015d, 2017) for mixtures of Athabasca bitumen with propane (C_3) and *n*-butane (C_4). The bitumen sample used for these papers is the same as that in Nourozieh et al. (2015b) for *n*-hexane. Liquid viscosities of propane and butane were estimated from saturated liquid viscosity reported in NIST. For supercritical temperatures, the Reynolds model for a single component was used to perform the extrapolation,

$$\mu_{\text{solvent}} = A\ \exp(-BT), \quad (12)$$

where A and B are two fitting parameters obtained from regression on NIST saturated liquid viscosities. Viscosity and temperature are measured in centipoise and degrees Celsius, respectively. A and B for C_3 are 0.1317 and 0.0124, and for C_4 are 0.2147 and 0.011. **Fig. 15** presents the result of regression to the NIST data for liquid C_3 and C_4. Then, the α-value for the modified Arrhenius equation is 0.36 for C_3 and 0.376 for C_4. The resulting modified Arrhenius correlation provides AARD of 54.4% and 17.4% for C_3/bitumen (Nourozieh et al. 2015d) and C_4/bitumen (Nourozieh et al. 2017), respectively.

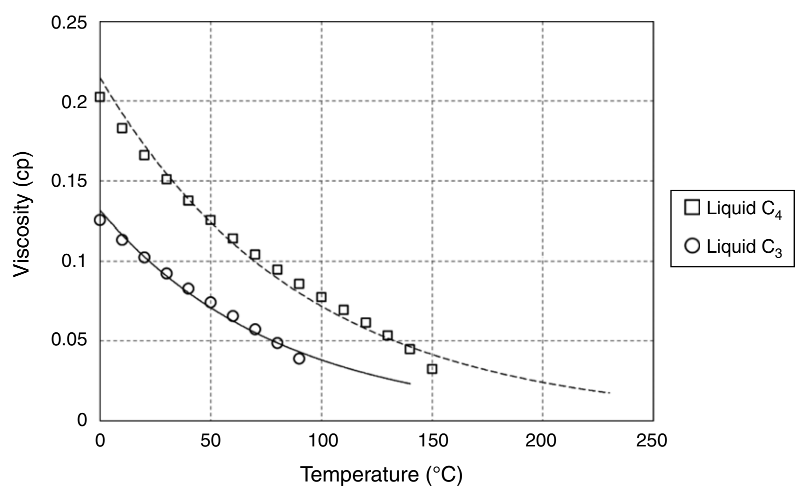

Fig. 15—Regression result with viscosities of liquid propane (C_3) and *n*-butane (C_4) given by NIST. *A* and *B* for Eq. 12 are 0.1317 and 0.0124 for C_3, and 0.2147 and 0.011 for C_4.

The viscosities of the mixtures of bitumen studied in this research with C_3, C_4, C_6, and DME are calculated using Eq. 7 along with the obtained α-values. **Fig. 16** presents the viscosity trends calculated at the solvent concentration of 50 mol% at 35 bar. The results show that the dilution of the bitumen is most significant with C_6. The other solvents are similar in terms of the capability of viscosity reduction at the 50-mol% dilution level.

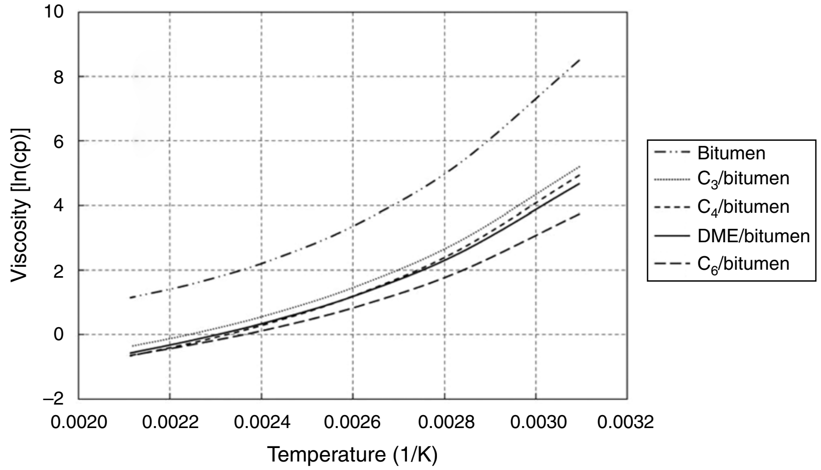

Fig. 16—Comparison between *n*-alkanes and DME in terms of bitumen dilution at 50 mol% solvent at 35 bar. The viscosities were calculated using the modified Arrhenius model developed in this research.

As described previously, a less-viscous solvent does not necessarily yield a lower viscosity when it is mixed with bitumen at a given molar concentration. Another point of discussion regarding DME is that the hydrogen bonding that can occur between DME and various components in the bitumen sample might cause the viscosity of the DME/bitumen mixture to increase.

Hansen (1967) considered that the total energy holding the liquid mixture together consists of the energy associated with dispersion, polarity, and hydrogen bonding,

$$\delta^2 = \delta_d^2 + \delta_p^2 + \delta_h^2, \quad (13)$$

where δ is the energy density (in 1/MPa). The subscripts *d, p,* and *h* represent the contributions of dispersion, polarity, and hydrogen bonding, respectively. The Hansen (1967) theory has been used to show the tendency of solvent interaction with polymers. Argillier et al. (2005) conducted a study of how intermolecular forces affect the capability of a solvent to dilute heavy oil using the Hansen (1967) dimensional solubility parameters. They concluded that a good solvent should have a high polarity parameter and a low hydrogen-bonding parameter. δ_p and δ_h values for commonly seen solvents were presented in Barton (1991). Alkanes have δ_p and δ_h of zero. Ether generally has a δ_p value from 3 to 5 and δ_h from 7 to 8. Methanol, which was reported by Argillier et al. (2005) to increase the viscosity of bitumen, has $\delta_p = 12$ and $\delta_h = 22$. In comparison, water has $\delta_p = 16$ and $\delta_h = 42$.

Results in this research showed that the DME/bitumen mixture is slightly more viscous than the *n*-hexane/bitumen mixture at the same concentration and at temperatures less than 380 K. This may be attributed to stronger intermolecular forces between DME and polar components in bitumen than those between *n*-hexane and bitumen. Complex compounds typically contained in bitumen include asphaltenes, which may form hydrogen bonds with DME molecules. At higher temperatures, the effect of hydrogen bonding on viscosity can be reduced, which might improve the capability of DME for viscosity reduction. This is in line with the observation that DME provides a similar level of viscosity reduction to *n*-hexane at higher temperatures (greater than 380 K). In contrast, no hydrogen bonding occurs between bitumen components and alkane solvents. Therefore, alkanes might perform well even at low temperatures, depending on the theory of Hansen (1967).

A good example for the effect of hydrogen bonding was reported by Dehaghani and Badizad (2016) for mixtures of methanol and a heavy oil, as shown in **Fig. 17.** In their study, viscosities of methanol/heavy-oil mixtures were measured to be clearly higher than the viscosity of 100% heavy oil. The authors attributed this viscosity increase to the self-association of methanol and the cross association between methanol and asphaltene molecules. The viscosities for their *n*-heptane/heavy-oil and methanol/heavy-oil mixtures were calculated from their reported kinematic viscosities and densities for Fig. 17.

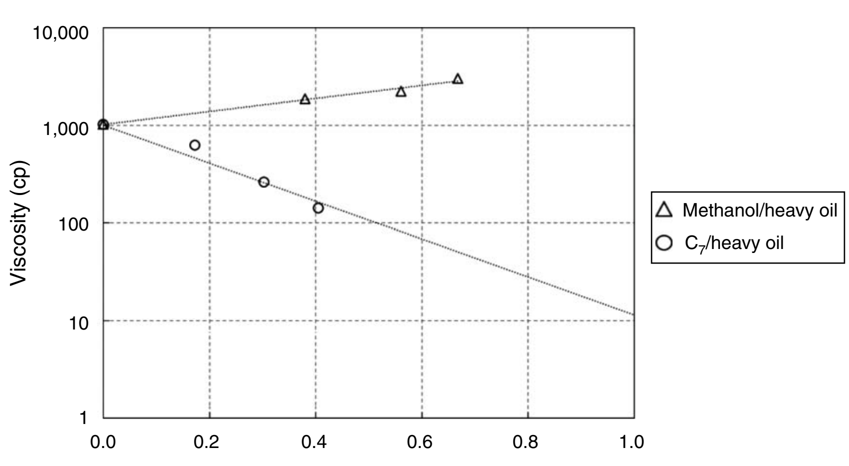

Fig. 17—Comparison of viscosities measured for *n*-heptane (C_7)/heavy-oil and methanol/heavy-oil mixtures by Dehaghani and Badizad (2016) at 293.15 K and atmospheric condition. The heavy oil has a value of °API 20. The viscosity is calculated from their reported kinematic viscosity, assuming the heavy-oil MW is 500 g/mol.

Conclusions

In this research, the capability of DME as a diluent for Athabasca bitumen was compared with that of *n*-hexane using measured viscosities and correlations. New experimental data were presented for phase behavior of Athabasca bitumen: five mixtures of Athabasca bitumen with DME and four mixtures of Athabasca bitumen with *n*-hexane. Our conclusions are as follows:

1. Liquid/liquid separation of solvent/bitumen mixtures, which occurred for *n*-butane/Athabasca bitumen in Gao et al. (2017), was not observed for any of the DME/bitumen and *n*-hexane/bitumen mixtures in this research. The highest solvent concentration in this study was 80 mol% DME (DB-1) for the DME/bitumen system and 92 mol% *n*-hexane (HB-2) for the *n*-hexane/bitumen system.
2. The Athabasca bitumen studied in this research was measured to be less viscous than the Athabasca bitumen studied by Nourozieh et al. (2015a, 2015b, 2015c, 2015d, 2017). Although the two bitumens are similar in terms of MW, the concentration of saturates in the bitumen studied in this research is twice as high as that of the other bitumen. This likely explains the lower viscosity of the bitumen studied in this research.
3. Three viscosity models were used to correlate the experimental data: a modified Arrhenius model, the power-law model, and the Walther (1931) model. In terms of AARD, the modified Arrhenius equation resulted in the best correlative accuracy among the three models. Although the Walther (1931) correlation provided a low AAD, it showed the largest AARD because of relatively large deviation for low-viscosity conditions. The power-law model was similar to the modified Arrhenius model for correlation of the *n*-hexane/bitumen mixtures, but it did not provide an accurate correlation for the DME/bitumen mixtures.
4. The modified Arrhenius equation with a weighting factor q_i as a function of α was able to capture the deviation of solvent/bitumen from the original Arrhenius (log-linear mixing) rule. It correlated well the viscosity data for the Athabasca bitumen diluted by *n*-hexane and DME. The relatively large α-value, 0.291, for the DME/bitumen mixtures compared with α of 0.0381 for the *n*-hexane/bitumen mixtures indicates that the viscosity of the DME/bitumen mixtures deviates more from the log-linear mixing rule.
5. The new experimental results showed that the equimolar mixture of DME with Athabasca bitumen was 79 cp and that of *n*-hexane with the same bitumen was 49 cp at 328 K and 60 bar. However, the two solvents were equivalent as diluent at temperatures greater than 380 K for the bitumen studied. For example, the difference was approximately 1 cp at 382 K and 35 bar between the equimolar mixture of Athabasca bitumen with DME and that with *n*-hexane. The new experimental data and viscosity correlations indicate that the dilution capability of DME becomes similar to that of *n*-hexane at higher-temperature and higher-solvent-concentration conditions.

Nomenclature

a_1 = coefficient in Eq. 2
a_2 = coefficient in Eq. 2
a_3 = coefficient in Eq. 2
a_4 = coefficient in Eq. 3
a_5 = coefficient in Eq. 3
A = coefficient in Eq. 12
b_1 = coefficient in Eq. 4
b_2 = coefficient in Eq. 4
b_3 = coefficient in Eq. 4
B = coefficient in Eq. 12
C = coefficient in Eq. 11
L = oleic phase
n = parameter in Eq. 10
P = pressure
q = weighting factor for L-phase viscosity (Eqs. 7, 8, and 9)
T = temperature
v = volume fraction
V = volume
W = aqueous phase
x = mole fraction
α = coefficient in Eq. 9
δ = energy density, 1/MPa
μ = viscosity, cp, mPa·s
ρ = density, kg/m^3

Subscripts

bit = bitumen
C_D = dead bitumen (Eq. 9)
d = dispersion (Eq. 13)
h = hydrogen bonding (Eq. 13)
L = oleic phase (Eqs. 7, 8, and 9)
p = polarity (Eq. 13)
s = solvent (Eqs. 10 and 11)

Acknowledgments

We gratefully acknowledge the financial support from Japan Canada Oil Sands Limited. Author Ryosuke Okuno holds the Pioneer Corporation Faculty Fellowship in Petroleum Engineering at the University of Texas at Austin. The authors thank Glen S. Baum for his assistance for this research.

References

Alkindi, A., Al-Azri, N., Said, D. et al. 2016. Persistence in EOR-Design of a Field Trial in a Carbonate Reservoir Using Solvent-Based Water-Flood Process. Presented at the SPE EOR Conference at Oil and Gas West Asia, Muscat, Oman, 21–23 March. SPE-179838-MS. https://doi.org/10.2118/179838-MS.

Argillier, J.-F., Henaut, I., Gateau, P. et al. 2005. Heavy Oil Dilution. Presented at the SPE International Thermal Operations and Heavy Oil Symposium, Calgary, 1–3 November. SPE-97763-MS. https://doi.org/10.2118/97763-MS.

Arrhenius, S. 1887. Über die Dissociation der in Wasser Gelösten Stoffe (On the Dissociation of Substances Dissolved in Water). *Z. Phys. Chem.* **1U** (1): 631–648. https://doi.org/10.1515/zpch-1887-0164.

ASTM D4006, Standard Test Method for Water in Crude Oil by Distillation. 2016. West Conshohocken, Pennsylvania: ASTM International.

Barton, A. F. 1991. *CRC Handbook of Solubility Parameters and Other Cohesion Parameters*, second edition. Boca Raton, Florida: CRC Press.

Chahardowli, M., Farajzadeh, R., and Bruining, H. 2016. Experimental Investigation of Dimethyl Ether/Polymer Hybrid as an Enhanced Oil Recovery Method. Presented at the SPE EOR Conference at Oil and Gas West Asia, Muscat, Oman, 21–23 March. SPE-179850-MS. https://doi.org/10.2118/179850-MS.

Chernetsky, A., Masalmeh, S., Eikmans, D. et al. 2015. A Novel Enhanced Oil Recovery Technique: Experimental Results and Modelling Workflow of the DME Enhanced Waterflood Technology. Presented at the Abu Dhabi International Petroleum Exhibition and Conference, Abu Dhabi, 9–12 November. SPE-177919-MS. https://doi.org/10.2118/177919-MS.

Computer Modelling Group (CMG). 2014. STARS Version 2014 User Guide. Calgary: CMG.

Dehaghani, A. H. S. and Badizad, M. H. 2016. Experimental Study of Iranian Heavy Crude Oil Viscosity Reduction by Diluting With Heptane, Methanol, Toluene, Gas Condensate and Naphtha. *Petroleum* **2** (4): 415–424. https://doi.org/10.1016/j.petlm.2016.08.012.

Gao, J., Okuno, R., and Li, H. A. 2017. An Experimental Study of Multiphase Behavior for *n*-Butane/Bitumen/Water Mixtures. *SPE J.* **22** (3): 783–798. SPE-180736-PA. https://doi.org/10.2118/180736-PA.

Gao, J., Okuno, R., and Li, H. A. 2018. A Phase-Behavior Study for *n*-Hexane/Bitumen and *n*-Octane/Bitumen Mixtures. *SPE J.* **23** (1): 128–144. SPE-186097-PA. https://doi.org/10.2118/186097-PA.

Gates, I. D. 2007. Oil Phase Viscosity Behavior in Expanding-Solvent Steam-Assisted Gravity Drainage. *J. Pet. Sci. Eng.* **59** (1–2): 123–134. https://doi.org/10.1016/j.petrol.2007.03.006.

Glandt, C. A. and Chapman, W. G. 1995. The Effect of Water Dissolution on Oil Viscosity. *SPE Res Eval & Eng* **10** (1): 59–64. SPE-24631-PA. https://doi.org/10.2118/24631-PA.

Groot, J. A. W. M., Eikmans, D., Fadili, A. et al. 2016a. Field-Scale Modelling and Sensitivity Analysis of DME Enhanced Waterflooding. Presented at the SPE EOR Conference at Oil and Gas West Asia, Muscat, Oman, 21–23 March. SPE-179798-MS. https://doi.org/10.2118/179798-MS.

Groot, J. A. W. M., Chernetsky, A., te Riele, P. M. et al. 2016b. Representation of Phase Behavior and PVT Workflow for DME Enhanced Water-Flooding. Presented at the SPE EOR Conference at Oil and Gas West Asia, Muscat, Oman, 21–23 March. SPE-179771-MS. https://doi.org/10.2118/179771-MS.

Gupta, S., Gittins, S., and Picherack, P. 2005. Field Implementation of Solvent Aided Process. *J Can Pet Technol* **44** (11): 8–13. PETSOC-05-11-TN1. https://doi.org/10.2118/05-11-TN1.

Gupta, S. C. and Gittins, S. D. 2006. Christina Lake Solvent Aided Process Pilot. *J Can Pet Technol* **45** (9): 15–18. PETSOC-06-09-TN. https://doi.org/10.2118/06-09-TN.

Haddadnia, A., Azinfar, B., Zirrahi, M. et al. 2018. Thermophysical Properties of Dimethyl Ether/Athabasca Bitumen System. *Can. J. Chem. Eng.* **96** (2): 597–604. https://doi.org/10.1002/cjce.23009.

Hansen, C. M. 1967. *The Three Dimensional Solubility Parameter and Solvent Diffusion Coefficient: Their Importance in Surface Coating Formulation*. Copenhagen, Denmark: Danish Technical Press.

Ihmels, E. C. and Lemmon, E. W. 2007. Experimental Densities, Vapor Pressures, and Critical Point, and a Fundamental Equation of State for Dimethyl Ether. *Fluid Phase Equilibr.* **260** (1): 36–48. https://doi.org/10.1016/j.fluid.2006.09.016.

Ivory, J. J., Zheng, R., Nasr, T. N. et al. 2008. Investigation of Low Pressure ES-SAGD. Presented at the International Thermal Operations and Heavy Oil Symposium, Calgary, 20–23 October. SPE-117759-MS. https://doi.org/10.2118/117759-MS.

Kariznovi, M., Nourozieh. H., Guan. J. et al. 2013. Measurement and Modeling of Density and Viscosity for Mixtures of Athabasca Bitumen and Heavy *n*-Alkane. *Fuel* **112** (October): 83–95. https://doi.org/10.1016/j.fuel.2013.04.071.

Keshavarz, M., Okuno, R., and Babadagli, T. 2014. Efficient Oil Displacement Near the Chamber Edge in ES-SAGD. *J. Pet. Sci. Eng.* **118** (June): 99–113. https://doi.org/10.1016/j.petrol.2014.04.007.

Keshavarz, M., Okuno, R., and Babadagli, T. 2015. Optimal Application Conditions for Steam/Solvent Coinjection. *SPE Res Eval & Eng* **18** (1): 20–38. SPE-165471-PA. https://doi.org/10.2118/165471-PA.

Leaute, R. P. and Carey, B. S. 2002. Liquid Addition to Steam for Enhancing Recovery (LASER) of Bitumen With CSS: Evolution of Technology From Research Concept to a Field Pilot at Cold Lake. Presented at the SPE International Thermal Operations and Heavy Oil Symposium and International Horizontal Well Technology Conference, Calgary, 4–7 November. PETSOC-2005-161. https://doi.org/10.2118/2005-161.

Li, W., Mamora, D. D., and Li, Y. 2011a. Light- and Heavy-Solvent Impacts on Solvent-Aided-SAGD Process: A Low-Pressure Experimental Study. *J Can Pet Technol* **50** (4): 19–30. SPE-133277-PA. https://doi.org/10.2118/133277-PA.

Li, W., Mamora, D. D., and Li, Y. 2011b. Solvent-Type and -Ratio Impacts on Solvent-Aided SAGD Process. *SPE Res Eval & Eng* **14** (3): 320–331. SPE-130802-PA. https://doi.org/10.2118/130802-PA.

Malkin, A. Y., Rodionova, G., Simon, S. et al. 2016. Some Compositional Viscosity Correlations for Crude Oils From Russia and Norway. *Energy Fuels* **30** (11): 9322–9328. https://doi.org/10.1021/acs.energyfuels.6b02084.

Mehrotra, A. K. and Svrcek, W. Y. 1986. Viscosity of Compressed Athabasca Bitumen. *Can. J. Chem. Eng.* **64** (5): 844–847. https://doi.org/10.1002/cjce.5450640520.

Michailidou, E. K., Assael, M. J., Huber. M. L. et al. 2013. Reference Correlation of the Viscosity of *n*-Hexane From the Triple Point to 600 K and Up to 100 MPa. *J. Phys. Chem. Ref. Data* **42** (3): 1–12. https://doi.org/10.1063/1.4818980.

Mohebati, M. H., Maini, B. B., and Harding, T. G. 2012. Numerical-Simulation Investigation of the Effect of Heavy-Oil Viscosity on the Performance of Hydrocarbon Additives in SAGD. *SPE Res Eval & Eng* **15** (2): 165–181. SPE-138151-PA. https://doi.org/10.2118/138151-PA.

Nasr, T. N., Beaulieu, G., Golbeck, H. et al. 2003. Novel Expanding Solvent-SAGD Process "ES-SAGD." *J Can Pet Technol* **42** (1): 13–16. PETSOC-03-01-TN. https://doi.org/10.2118/03-01-TN.

Nourozieh, H., Kariznovi, M., Guan, J. G. et al. 2013. Measurement of Thermophysical Properties and Modeling for Pseudo-Binary Mixtures of *n*-Decane and Athabasca Bitumen. *Fluid Phase Equilibr.* **347** (15 June): 62–75. https://doi.org/10.1016/j.fluid.2013.03.010.

Nourozieh, H., Kariznovi, M., and Abedi, J. 2015a. Density and Viscosity of Athabasca Bitumen Samples at Temperatures Up to 200°C and Pressures Up to 10 MPa. *SPE J.* **18** (3): 375–386. SPE-176026-PA. https://doi.org/10.2118/176026-PA.

Nourozieh, H., Kariznovi, M., and Abedi, J. 2015b. Viscosity Measurement and Modeling for Mixtures of Athabasca Bitumen/Hexane. *J. Pet. Sci. Eng.* **129** (May): 159–167. https://doi.org/10.1016/j.petrol.2015.03.002.

Nourozieh, H., Kariznovi, M., and Abedi, J. 2015c. Viscosity Measurement and Modeling for Mixtures of Athabasca Bitumen/*n*-Pentane at Temperatures Up to 200°C. *SPE J.* **20** (2): 226–238. SPE-170252-PA. https://doi.org/10.2118/170252-PA.

Nourozieh, H., Kariznovi, M., and Abedi, J. 2015d. Experimental and Modeling Studies of Phase Behavior for Propane/Athabasca Bitumen Mixtures. *Fluid Phase Equilibr.* **397** (15 July): 37–43. https://doi.org/10.1016/j.fluid.2015.03.047.

Nourozieh, H., Kariznovi, M., and Abedi, J. 2017. Solubility of *n*-Butane in Athabasca Bitumen and Saturated Densities and Viscosities at Temperatures Up to 200°C. *SPE J.* **22** (1): 94–102. SPE-180927-PA. https://doi.org/10.2118/180927-PA.

Parsons, C., Chernetsky, A., Eikmans, D. et al. 2016. Introducing a Novel Enhanced Oil Recovery Technology. Presented at the SPE Improved Oil Recovery Conference, Tulsa, 11–13 April. SPE-179560-MS. https://doi.org/10.2118/179560-MS.

Ramos-Pallares, F., Schoeggl, F. F., Taylor, S. D. et al. 2015. Predicting the Viscosity of Hydrocarbon Mixtures and Diluted Heavy Oils Using the Expanded Fluid Model. *Energy Fuels* **30** (5): 3575–3595. https://doi.org/10.1021/acs.energyfuels.5b01951.

Shen, C. 2013. *Enhanced Oil Recovery Field Case Studies*, first edition. New York City: Elsevier.

Sheng, K., Okuno, R., and Wang, M. 2018. Dimethyl Ether as an Additive to Steam for Improved Steam-Assisted Gravity Drainage. *SPE J* **23** (4): 1201–1222. SPE-184983-PA. https://doi.org/10.2118/184983-PA.

te Riele, P., Parsons, C., Boerrigter, P. et al. 2016. Implementing a Water Soluble Solvent Based Enhanced Oil Recovery Technology-Aspects of Field Development Planning. Presented at the SPE EOR Conference at Oil and Gas West Asia, Muscat, Oman, 21–23 March. SPE-179849-MS. https://doi.org/10.2118/179849-MS.

Venkatramani, A. V. and Okuno, R. 2017. Compositional Mechanisms in Steam-Assisted Gravity Drainage and Expanding-Solvent Steam-Assisted Gravity Drainage With Consideration of Water Solubility in Oil. *SPE Res Eval & Eng* **20** (3): 681–697. SPE-180737-PA. https://doi.org/10.2118/180737-PA.

Venkatramani, A. V. and Okuno, R. 2018. Mechanistic Simulation Study of Expanding-Solvent Steam-Assisted Gravity Drainage Under Reservoir Heterogeneity. *J. Pet. Sci. Eng.* **169** (October): 146–156. https://doi.org/10.1016/j.petrol.2018.04.074.

Walther, C. 1931. The Evaluation of Viscosity Data. *Erdol Teer* **7:** 382–384.

Wu, J. and Yin, J. 2008. Vapor Pressure Measurements of Dimethyl Ether From (213 to 393) K. *J. Chem. Eng. Data* **53** (9): 2247–2249. https://doi.org/10.1021/je800375t.

Wu, J., Liu, Z., Bi, S. et al. 2003. Viscosity of Saturated Liquid Dimethyl Ether From (227 to 343) K. *J. Chem. Eng. Data* **48** (2): 426–429. https://doi.org/10.1021/je0256232.

Wu, J., Liu, Z., Wang, B. et al. 2004. Measurement of the Critical Parameters and the Saturation Densities of Dimethyl Ether. *J. Chem. Eng. Data* **49** (3): 704–708. https://doi.org/10.1021/je034251+.

Zhu, D. and Okuno, R. 2016. Multiphase Isenthalpic Flash Integrated With Stability Analysis. *Fluid Phase Equilibr.* **423** (15 September): 203–219. https://doi.org/10.1016/j.fluid.2016.04.005.

Zou, X.-Y., Zhang, X., and Shaw, J. A. M. 2007. Phase Behavior of Athabasca Vacuum Bottoms + *n*-Alkane Mixtures. *SPE Prod & Oper* **22** (2): 265–272. SPE-97661-PA. https://doi.org/10.2118/97661-PA.

Kwang Hoon Baek is a PhD degree candidate in petroleum engineering in the Hildebrand Department of Petroleum and Geosystems Engineering at the University of Texas at Austin. His research interests include thermal enhanced oil recovery (EOR), chemical EOR, multiphase behavior, and fluid properties of petroleum fluids. Baek holds a bachelor's degree in chemical engineering from Yonsei University, South Korea, and a master's degree in science and technology policy from Korea Advanced Institute of Science and Technology. He is a member of SPE.

Kai Sheng is a PhD degree candidate in petroleum engineering in the Hildebrand Department of Petroleum and Geosystems Engineering at the University of Texas at Austin. His research interests include thermal EOR, numerical reservoir simulation, and multiphase behavior and fluid properties of heavy oil and bitumen. Sheng holds a bachelor's degree from the China University of Petroleum, East China, and a master's degree from the University of Alberta, Canada, both in petroleum engineering. He is a member of SPE.

Francisco Javier Argüelles-Vivas is a post-doctoral-degree fellow in the Hildebrand Department of Petroleum and Geosystems Engineering at the University of Texas at Austin. Previously, he worked as a reservoir engineer at the Mexican Petroleum Institute for 2 years. Argüelles-Vivas' current research interests are EOR methods for conventional/unconventional reservoirs, formation damage, phase behavior of bitumen/heavy-oil/solvent mixtures, pore-scale modeling, and carbon dioxide sequestration. He holds a bachelor's degree in chemical engineering from the Metropolitan Autonomous University, Mexico; a master's degree in petroleum engineering from the Mexican Petroleum Institute; and a PhD degree in petroleum engineering from the University of Alberta. Argüelles-Vivas is a member of SPE and currently serves as a technical reviewer for *SPE Journal*.

Ryosuke Okuno is an associate professor in the Hildebrand Department of Petroleum and Geosystems Engineering and holds the Pioneer Corporation Faculty Fellowship in Petroleum Engineering at the University of Texas at Austin. Before his current position, he served as an assistant professor of petroleum engineering in the Department of Civil and Environmental Engineering at the University of Alberta from 2010 to 2015. Okuno also holds 7 years of industrial experience as a reservoir engineer with Japan Petroleum Exploration Company Limited, and is a registered professional engineer in Alberta, Canada. His research and teaching interests include EOR, thermal oil recovery, unconventional oil and gas, numerical reservoir simulation, thermodynamics, multiphase behavior, and applied mathematics. Okuno holds bachelor's and master's degrees in geosystem engineering from the University of Tokyo and a PhD degree in petroleum engineering from the University of Texas at Austin. He is a recipient of the 2012 SPE Petroleum Engineering Junior Faculty Research Initiation Award and is an associate editor for *SPE Journal*.